1D modeling of a flowing electrolyte-direct methanol fuel cell

C. Ozgur Colpan [a,*], Cynthia Ann Cruickshank [a], Edgar Matida [a], Feridun Hamdullahpur [b]

[a] Mechanical and Aerospace Engineering Department, Carleton University, 1125 Colonel by Drive, Ottawa, Ontario, Canada K1S 5B6
[b] Mechanical and Mechatronics Engineering Department, University of Waterloo, 200 University Avenue West, Waterloo, Ontario, Canada N2L 3G1

ARTICLE INFO

ABSTRACT

In this study, the performance characteristics of a flowing electrolyte-direct methanol fuel cell (FE-DMFC) and a direct methanol fuel cell (DMFC) are evaluated by computer simulations; and results are compared to experimental data found in the literature. Simulations are carried out to assess the effects of the operating parameters on the output parameters; namely, methanol concentration distribution, cell voltage, power density, and electrical efficiency of the cell. The operating parameters studied include the electrolyte flow rate, flowing electrolyte channel thickness, and methanol concentration at the feed stream. In addition, the effect of the circulation of the flowing electrolyte channel outlet stream on the performance is discussed. The results show that the maximum power densities that could be achieved do not significantly differ between these two fuel cells; however the electrical efficiency could be increased by 57% when FE-DMFC is used instead of DMFC.

© 2010 Elsevier B.V. All rights reserved.

1. Introduction

Direct methanol fuel cells (DMFCs) are a promising technology to produce power for small-scale applications. DMFCs are a subset of PEM (polymer electrolyte membrane) fuel cells and have relatively low operating temperatures in the range of 50–120 °C. The low-temperature oxidation of methanol requires a more active catalyst with a larger quantity of the relatively expensive platinum (Pt). Methanol (CH_3OH) is electrochemically oxidized at the anode (negative electrode, having Pt and ruthenium, Ru as catalysts), producing electrons, which travel through the external circuit to the cathode (positive electrode, having Pt) where they are consumed together with oxygen in a reduction reaction. The circuit is maintained within the cell by the conduction of protons in the electrolyte (normally a polymer electrolyte membrane, PEM, for example Nafion®). Active (i.e., controlled air and fuel flows) and passive (i.e., natural flow of air) DMFCs are expected to penetrate the market to provide power to devices such as cell phones, laptops, digital cameras, LCD-TVs, and MP3 players. In the current state-of-art, when compared to Li-ion batteries, DMFCs are more advantageous in terms of size and weight when they are designed to be used for longer operating times [1].

One of the shortcomings of DMFCs is the unwanted crossover of methanol from the anode to cathode during operation. This methanol crossover leads to a reduction in the power density and the electrical efficiency of the cell. To minimize the effects of this crossover, strategies such as controlling the operating parameters, e.g. inlet methanol concentration, and using alternative materials for the components of the cell are generally considered [1]. In addition to the methanol crossover problem, the other challenges with DMFCs are low activation polarization of the anode, and water and heat management issues [2].

In order to circumvent the issue of the methanol crossover (from the anode to the cathode through the PEM), Kordesch et al. [3–5] proposed a novel DMFC concept by introducing a flowing electrolyte (e.g., diluted sulfuric acid, $H_2SO_4 + H_2O$), reducing the methanol crossover from the electrolyte compartment by means of convection mechanisms (the methanol is carried away without contaminating the cathode). In their suggested design, the flowing electrolyte was pumped to the cell (through the electrolyte channel separating the anode and cathode) and also re-circulated, thus forming a "circulating electrolyte-direct methanol fuel cell". In the present work, the term "flowing electrolyte" implies that the electrolyte is not being re-circulated. Practically, fresh electrolyte would be used and the methanol-contaminated electrolyte would be stored in a container. The contaminated electrolyte would be retrieved and recycled in separate industrial facilities using distillation or membrane separation processes. It is likely that in situ recycling (at the FE-DMFC unit) may not be viable when compactness is desired. Alternatively, the contaminated electrolyte could also be pumped through an additional DMFC unit, where the methanol in the methanol-contaminated electrolyte would be consumed (co-generation concept). There has been some effort in the

* Corresponding author. Tel.: +1 416 979 5000x7833; fax: +1 613 520 5715.
E-mail addresses: cocolpan@connect.carleton.ca, ozgurcolpan@yahoo.com
(C.O. Colpan).

Nomenclature

b	width of the flowing electrolyte channel (cm)
C	concentration, (mole cm^{-3})
D	coefficient of diffusion (cm^2 s^{-1})
F	Faraday's constant (s A mole^{-1})
j	current density (A cm^{-2})
j_o	exchange current density (A cm^{-2})
j_{lim}	limiting current density (A cm^{-2})
j_{xover}	crossover current density (A cm^{-2})
n_d	electro-osmotic drag coefficient
K	equation constant
L	length (cm)
$\overline{LHV}$	lower heating value in molar basis (J mole^{-1})
n	reaction order
$\dot{N}''$	molar flow rate per cross section (mole cm^{-2} s^{-1})
P	pressure (atm)
R	universal gas constant (J K^{-1} mole^{-1})
t	thickness (cm)
T	temperature of the cell (K)
u_{eo}	velocity due to electro-osmosis in the thickness direction (cm s^{-1})
v_{FEC}	velocity of the flowing electrolyte in the longitudinal direction (cm s^{-1})
V	voltage (V)
$\dot{V}$	electrolyte flow rate (cm^3 s^{-1})
x	distance (cm)
$\dot{W}''_{cell}$	power density of the cell (W cm^{-2})

Greek letters

α	transfer coefficient
ε	porosity
σ	conductivity (S cm^{-1})
η	polarization (V)
η_{el}	electrical efficiency of the cell
υ	number of protons produced or consumed per one mol of reactant

Subscripts

act	activation
conc	concentration
OCV	open circuit voltage
ohm	ohmic
rev	reversible
xover	crossover

Superscripts

a	anode
ABL	anode backing layer
ACL	anode catalyst layer
AM	anode membrane
c	cathode
CBL	cathode backing layer
CCL	cathode catalyst layer
CM	cathode membrane
FEC	flowing electrolyte channel
ref	reference

relations to find the performance of the cell. The level of coverage of the detailed mechanisms in the fuel cell and the solution of the modeling equations vary among these models. For example, Kulikovsky [12] developed several 1D and quasi 2D analytical or semi-analytical DMFC models. In these models, the effects of diffusive transport of methanol and oxygen through a cell, gaseous bubbles formation in the anode channel, and the non-Tafel kinetics of methanol oxidation on the anode catalyst layer performance were studied. Liu et al. [13] and Wang [14] discussed the influence of water transport in methanol crossover; and found out that water transport has to be considered as one of the most important aspects of the DMFC modeling. Ge and Liu [15] developed a three dimensional, single phase, multi-component mathematical model, and used a finite-volume based computational fluid dynamics (CFD) model for the solution. Wang and Wang [16] developed a two-dimensional, two-phase, multi-component DMFC model using a CFD technique. Garcia et al. [17] included the kinetics of the multi-step methanol oxidation reaction at the anode to their one-dimensional, isothermal, and semi-analytical model. Finally, in the study by Oliveira et al. [18], the heat transfer effects were included in a one-dimensional CFD model to obtain the temperature distribution through the cell as well as other output such as cell voltage.

Unlike the numerous DMFC models found in the literature, there are only two modeling studies on FE-DMFCs [9,10]. The main objective of these studies was to find the reduction of methanol crossover with different operating parameters rather than to find the overall performance of a single cell. Due to the lack of complete modeling studies on the FE-DMFCs in the literature, a 1D model has been developed to study the effects of the operating parameters such as electrolyte flow rate, flowing electrolyte channel thickness, and methanol concentration at the feed stream on the performance of a FE-DMFC. In addition, a DMFC model has been developed to allow direct comparisons between the performances of DMFCs and FE-DMFCs. In these models, methanol, water, and oxygen transport equations are integrated with the electrochemical relations to find the concentration distribution of the species through the cell, and to obtain the cell voltage, the power density, and the electrical efficiency of the cell. The model is validated using DMFC data found in the literature.

2. Modeling

This section includes the approach, assumptions, equations, and solution method used in the modeling of a DMFC and a FE-DMFC. The main components and reactions of a DMFC and a FE-DMFC are shown in Figs. 1 and 2, respectively. As can be seen in these figures, unlike the DMFC, the FE-DMFC consists of two membranes mainly used to separate the flowing electrolyte channel from the active catalyst layers. In the flowing electrolyte channel, the methanol crossed over is washed away from the cell. Discussions on the operation of these fuel cells are given in the following subsections.

2.1. Modeling approach and assumptions

One dimensional models of a DMFC and a FE-DMFC have been developed. In these models, species transport equations by diffusion and electro-osmosis have been integrated with electrochemistry relations. The flow chart of the model developed is shown in Fig. 3. As can be seen in this figure, several constants, geometry of the cell, operating parameters, and material properties are taken as input. The species transport equations are solved in the following sequence: water, methanol, and oxygen transport. As a result of solving the transport equations, we find the concentration and molar flow rate of the species in the thickness direction. These findings are used to solve the electrochemistry relations to
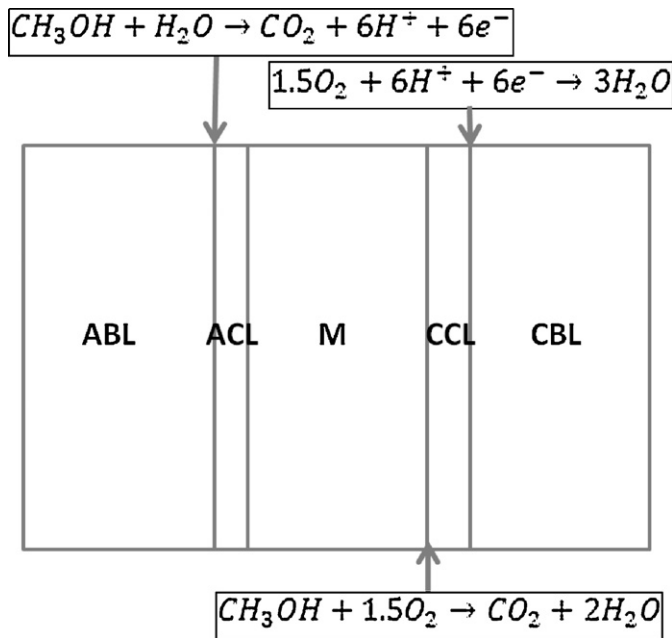
development of FE-DMFCs in the last decade [6–11]. Possible applications of FE-DMFC may include backup power for recreational activities, golf cars, forklifts, and unmanned aerial vehicle.

Several studies on DMFC modeling have appeared in the literature. In the majority of these studies, the mass transport in the different layers of a single cell is coupled with the electrochemical

$$CH_3OH + H_2O \rightarrow CO_2 + 6H^+ + 6e^-$$

$$1.5O_2 + 6H^+ + 6e^- \rightarrow 3H_2O$$

| ABL | ACL | M | CCL | CBL |

$$CH_3OH + 1.5O_2 \rightarrow CO_2 + 2H_2O$$

Fig. 1. Schematic of a DMFC (ABL: anode backing layer, ACL: anode catalyst layer, M: membrane, CCL: cathode catalyst layer, and CBL: cathode backing layer).

form the polarization, power density, and cell efficiency curves.

The main assumptions of the models are as follows:

- concentrations of the species are constant at the catalyst layers;
- methanol is fully consumed at the cathode catalyst layer;
- the reactions are heterogeneous, i.e., they are treated as a surface phenomenon;
- the change of conductivities of the membrane and flowing electrolyte with space is neglected;
- the formations of CO_2 bubbles and water vapour are neglected; i.e., only liquid phase is considered at the anode side;
- membranes are fully hydrated;
- the effects due to the channel curvature are not taken into account;
- the flow in the electrolyte channel is considered as fully developed laminar flow;
- the fuel cell is isothermal; and
- the fuel cell operates at steady state condition.

2.2. Modeling equations

The species transport equations (i.e., water, methanol, and oxygen transport) and electrochemistry relations (i.e., ohmic, activation, and concentration polarizations) for a DMFC and a FE-DMFC are presented in this section. In the modeling equations, numbers are used as subscripts to indicate the locations. These numbers and their corresponding locations are shown in Table 1. Please note that

Table 1
Numbering scheme used in the modeling.

Point	Interface
1	Fuel channel and anode backing layer (ABL)
2	Anode backing layer (ABL) and anode catalyst layer (ACL)
3	Anode catalyst layer (ACL) and anode membrane (AM)
4	Anode membrane (AM) and flowing electrolyte channel (FEC)
5	Flowing electrolyte channel (FEC) and cathode membrane (CM)
6	Cathode membrane (CM) and cathode catalyst layer (CCL)
7	Cathode catalyst layer (CCL) and cathode backing layer (CBL)
8	Cathode backing layer (CBL) and air channel

unless otherwise stated, the equations shown in this section are valid for both DMFC and FE-DMFC.

2.2.1. Water transport

Water first diffuses from the fuel channel to the ACL; and then transports to the other layers due to electro-osmosis. Electro-osmotic drag coefficient can be defined as the number of water molecules dragged per the number of proton molecules produced, as shown in Eq. (1).

$$n_d = \frac{\dot{N}''_{H_2O}}{\dot{N}''_{H^+}} = \frac{\dot{N}''_{H_2O}}{j/F} \tag{1}$$

If we take a control volume around the ABL, we can show that the molar flow rate of water entering the ACL is equal to the summation of the amount of water consumed at the electrochemical reaction occurring at the ACL and water crossing over to the membrane.

$$-D^{ABL}_{H_2O} \frac{\partial C^{ABL}_{H_2O}}{\partial x} = \frac{j}{6F} + \dot{N}''_{xover,H_2O} \tag{2}$$

Combining Eqs. (1) and (2), and solving them analytically, we can find the concentration of the water at the ACL.

$$C^{ACL}_{H_2O} = C_{1,H_2O} - \left[\frac{(n_d + 1/6) \cdot j}{D^{ABL}_{H_2O} \cdot F} \right] \cdot (x_2 - x_1) \tag{3}$$

2.2.2. Methanol transport

As one of the modeling objectives is to find the methanol concentration in the thickness direction, the governing equations and boundary conditions are shown for each control volume enclosing the layers of a cell. Please note that CH_3OH subscript is not shown in this section for convenience.

Methanol first diffuses from the fuel channel to the ACL through the ABL. Then, some amount of it is spent in the electrochemical reaction occurring at the ACL, and the remaining crosses over to the anode membrane. The governing equation and boundary conditions of the ABL are as follows:

$$\frac{\partial^2 C^{ABL}}{\partial x^2} = 0 \tag{4}$$

$$\text{At } x = x_1 : C = C_1 \tag{4.1}$$

$$\text{At } x = x_2 : -D^{ABL} \frac{\partial C^{ABL}}{\partial x}|_{x=x_2} = \frac{j}{6F} + \dot{N}''_3 \tag{4.2}$$

Eq. (4) can be solved analytically; and can be shown as follows:

$$C^{ABL} = K_1 x + K_2 \tag{5}$$

Methanol is transported due to diffusion and electro-osmosis through the membrane of DMFC or anode membrane of FE-DMFC. The amount of methanol dragged due to electro-osmosis is shown in Eq. (6)

$$\dot{N}'' = N''_{H_2O} \cdot \frac{C}{C_{H_2O}} = n_d \cdot \frac{j}{F} \cdot \frac{C}{C_{H_2O}} \tag{6}$$

Here, we define x-component velocity due to electro-osmosis as shown in Eq. (7).

$$u_{eo} = \frac{n_d \cdot j}{F \cdot C^{ACL}_{H_2O}} \tag{7}$$

The governing equation and the boundary conditions of the anode membrane are shown below. It should be noted that the methanol concentration reaching the CCL is zero for a DMFC; because it is assumed that methanol is fully oxidized at this point
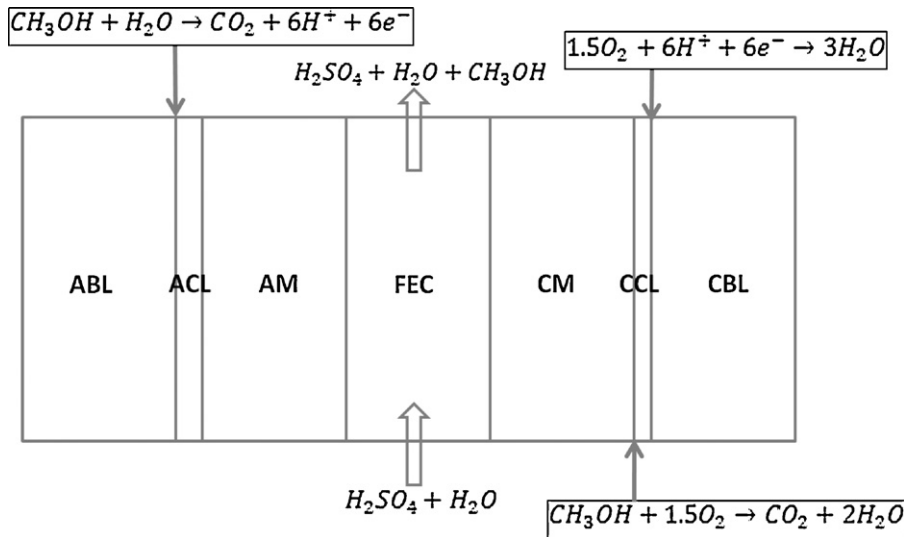
$$CH_3OH + H_2O \rightarrow CO_2 + 6H^+ + 6e^-$$

$$H_2SO_4 + H_2O + CH_3OH$$

$$1.5O_2 + 6H^+ + 6e^- \rightarrow 3H_2O$$

ABL ACL AM FEC CM CCL CBL

$$H_2SO_4 + H_2O$$

$$CH_3OH + 1.5O_2 \rightarrow CO_2 + 2H_2O$$

Fig. 2. Schematic of a FE-DMFC (ABL: anode backing layer, ACL: anode catalyst layer, AM: anode membrane, FEC: flowing electrolyte channel, CM: cathode membrane, CCL: cathode catalyst layer, and CBL: cathode backing layer).

considering that catalyst is abundant at the CCL and no significant water flooding happens.

$$D^{AM} \frac{\partial^2 C^{AM}}{\partial x^2} - u_{eo} \frac{\partial C^{AM}}{\partial x} = 0 \qquad (8)$$

At $x = x_3 : \dot{N}_3'' = -D^{AM} \frac{\partial C^{AM}}{\partial x}\big|_{x=x_3} + u_{eo} \cdot C_3 \qquad (8.1)$

At $x = x_4$ (for DMFC) $: C_4 = 0 \qquad (8.2)$

At $x = x_4$ (for FE-DMFC) $: \dot{N}_4'' = -D^{AM} \frac{\partial C^{AM}}{\partial x}\big|_{x=x_4} + u_{eo} \cdot C_4 \qquad (8.3)$

The methanol distribution in the anode membrane can be found by solving Eq. (8) analytically as follows:

$$C^{AM} = K_3 + K_4 \cdot e^{(u_{eo} \cdot x)/D^{AM}} \qquad (9)$$

In a FE-DMFC, methanol passes through the flowing electrolyte channel due to diffusion and electro-osmosis mechanisms; but also washes away from the cell with the flowing electrolyte. The velocity of the flowing electrolyte in the longitudinal direction has been

derived for a fully developed laminar flow after using the findings of the study by White [19], and doing some mathematical manipulations.

$$v_{FEC}(x) = \frac{6 \cdot \dot{V} \cdot (x - x_4) \cdot (x_5 - x)}{b \cdot (x_5 - x_4)^3} \qquad (10)$$

The governing equation and the boundary conditions for the FEC can be shown as follows:

$$D^{FEC} \frac{\partial^2 C^{FEC}}{\partial x^2} - u_{eo} \frac{\partial C^{FEC}}{\partial x} - \frac{v_{FEC}(x) \cdot C^{FEC}}{L_{FEC}} = 0 \qquad (11)$$

At $x = x_4 : \dot{N}_4'' = -D^{FEC} \frac{\partial C^{FEC}}{\partial x}\big|_{x=x_4} + u_{eo} \cdot C_4 \qquad (11.1)$

At $x = x_5 : \dot{N}_5'' = -D^{FEC} \frac{\partial C^{FEC}}{\partial x}\big|_{x=x_5} + u_{eo} \cdot C_5 \qquad (11.2)$

A finite difference method can be applied to convert Eq. (11) to a set of linear equations. For this purpose, central finite difference for the interior nodes, forward and backward difference for the boundary conditions at x_4 and x_5 can be applied, respectively.

INPUT
Constants
Geometry of the Cell
Operating Parameters
Material Properties

LOGIC
Water Transport
Methanol Transport
Oxygen Transport
Electro-chemistry

OUTPUT
Concentration distributions
Polarization curve
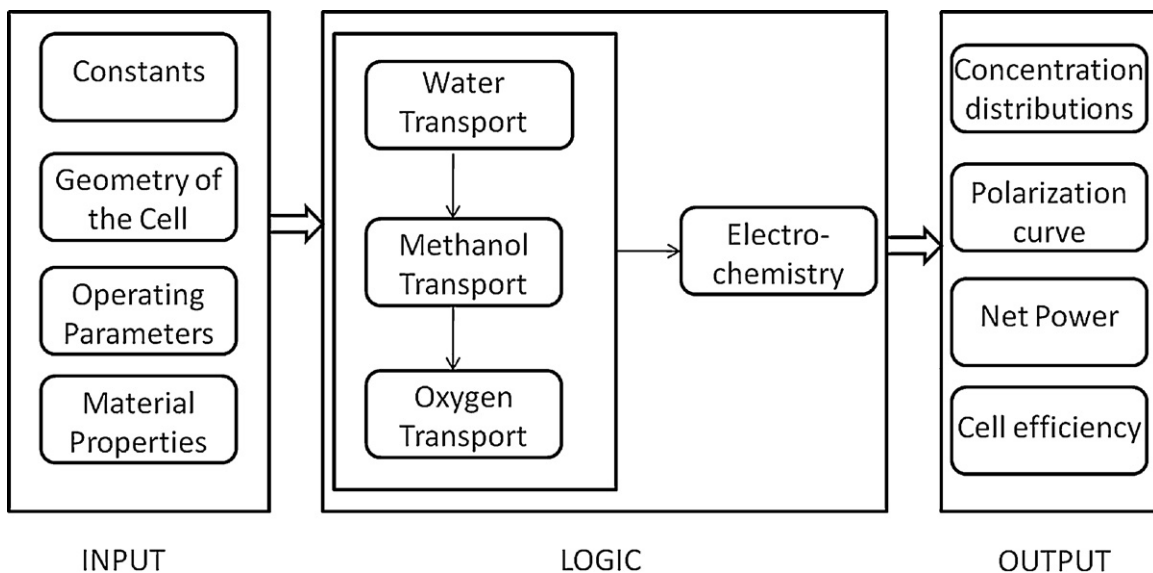Net Power
Cell efficiency

Fig. 3. The flow chart of the models.

For a FE-DMFC, depending on the flow rate of the flowing electrolyte, some amount of methanol may pass through the cathode membrane or all of the methanol may be washed away from the cell. In either condition, we can show the governing equation and boundary conditions for the CM as follows:

$$D^{CM}\frac{\partial^2 C^{CM}}{\partial x^2} - u_{eo}\frac{\partial C^{CM}}{\partial x} = 0 \tag{12}$$

$$\text{At } x = x_5 : \dot{N}_5'' = -D^{CM}\frac{\partial C^{CM}}{\partial x}|_{x=x_5} + u_{eo}\cdot C_5 \tag{12.1}$$

$$\text{At } x = x_6 : C_6 = 0 \tag{12.2}$$

The methanol concentration distribution at the CM can be shown as Eq. (13) after solving Eq. (12) analytically.

$$C^{CM} = K_5 + K_6 \cdot e^{(u_{eo}\cdot x)/D^{CM}} \tag{13}$$

After eliminating the common terms between the boundary conditions, e.g. $\dot{N}_3''$ between Eqs. (4.2) and (8.1), and rearranging the equations; the number of equations can be reduced and shown as a set of linear equations. For the DMFC model, the equations can be reduced to 4 equations with 4 unknowns (i.e., K_1 to K_4). For the FE-DMFC model, the number of equations can be reduced to $n + 6$ with $n + 6$ unknowns, where n is the number of unknowns indicating the methanol concentration at each interior node of the FEC and 6 is the number of unknowns for K terms (i.e., K_1 to K_6). Once the K terms are found using the Gauss elimination method, methanol concentration at the ABL, AM, and CM can be found using Eqs. (5), (9), and (13), respectively. Since the methanol concentration at each interior node at the FEC is an unknown, the methanol distribution at this layer is found directly by the solution of the set of linear equations.

2.2.3. Oxygen transport

The oxygen found in the air channel diffuses through the CBL, and then spent in the electrochemical reaction and the oxidation of the crossover methanol reaction occurring at the CCL. If we take a control volume around the CBL, we can write the amount of oxygen diffused through the CBL as follows:

$$D_{O_2}^{CBL}\frac{\partial C_{O_2}^{CBL}}{\partial x} = \frac{j}{4F} + \frac{3}{2}\dot{N}_{xover,CH_3OH}'' \tag{14}$$

where $\dot{N}_{xover,CH_3OH}''$ is the amount of methanol reaching the CCL. Oxygen concentration at the CCL may be found by solving Eq. (14) analytically as follows:

$$C_{O_2}^{CCL} = C_{8,O_2} - \left[\frac{\frac{j}{4F} + \frac{3}{2}\dot{N}_{xover,CH_3OH}''}{D_{O_2}^{CBL}}\right]\cdot(x_8 - x_7) \tag{15}$$

2.2.4. Electrochemistry

The reversible open circuit voltage in a DMFC is 1.21 V [20]. However, due to the methanol crossover, lower open circuit voltage is achieved; and due to the ohmic, activation, and concentration polarizations, cell voltage also drops. The cell voltage can be shown as follows:

$$V_{cell} = V_{OCV,rev} - \eta_{act} - \eta_{ohm} - \eta_{conc} \tag{16}$$

Activation polarization is caused by the sluggishness of the reactions. Using the Tafel equation, anodic activation polarization can be calculated as follows:

$$\eta_{act}^a = \left(\frac{R\cdot T}{\alpha_a \cdot F}\right)\cdot \ln\left(\frac{j}{j_{oa}}\right) \tag{17}$$

In Eq. (17), exchange current density of anode can be calculated using the measurements done with reference electrodes [16]

$$j_{oa} = j_{oa}^{ref}\left(\frac{C_{CH_3OH}}{C_{CH_3OH}^{ref}}\right)^n \tag{17.1}$$

where

$$n = \begin{cases} 0 : C_{CH_3OH} \geq C_{CH_3OH}^{ref} \\ 1 : C_{CH_3OH} < C_{CH_3OH}^{ref} \end{cases} \tag{17.2}$$

At the cathode, because of the oxidation of the crossover methanol, oxygen concentration drops and some portion of the active catalyst areas are covered by methanol; which causes a mixed potential. Cathodic activation polarization can be calculated as follows:

$$\eta_{act}^c = \left(\frac{R.T}{\alpha_c \cdot F}\right)\cdot \ln\left(\frac{j + j_{xover}}{j_{oc}}\right) \tag{18}$$

In Eq. (18), exchange current density of cathode and crossover current density may be found using Eqs. (18.1) and (18.2), respectively.

$$j_{oc} = j_{oc}^{ref}\frac{P_{O_2}}{P_{O_2}^{ref}} \tag{18.1}$$

$$j_{xover} = 6\cdot F \cdot \dot{N}_{xover,CH_3OH}'' \tag{18.2}$$

Ohmic polarization is caused by the resistance to the ions and electrons, and also due to the contact between the components. This polarization can be approximated using Ohm's law as follows:

$$\eta_{ohm} \cong \left(\frac{t^{AM}}{\sigma^{AM}} + \frac{t^{FEC}}{\sigma^{FEC}} + \frac{t^{CM}}{\sigma^{CM}}\right)\cdot j \tag{19}$$

Concentration polarization in DMFCs is generally negligible; but they could be still included in modeling to have more accurate results. This polarization at the anode can be estimated as follows:

$$\eta_{conc}^a = \left(\frac{-R.T}{\nu_a \cdot F}\right)\cdot \ln\left(1 - \frac{j}{j_{lim,a}}\right) \tag{20}$$

where the limiting current density at the anode can be calculated as

$$j_{lim,a} = \frac{6\cdot F \cdot D_{CH_3OH}^{ABL}\cdot C_{1,CH_3OH}}{t^{ABL}} \tag{20.1}$$

The concentration polarization at the cathode can be calculated as follows:

$$\eta_{conc}^c = \left(\frac{-R.T}{\nu_c \cdot F}\right)\cdot \ln\left(1 - \frac{j}{j_{lim,c}}\right) \tag{21}$$

where the limiting current density at the cathode can be calculated as

$$j_{lim,c} = \frac{4\cdot F \cdot D_{O_2}^{CBL}\cdot C_{8,O_2}}{t^{CBL}} \tag{21.1}$$

After finding the ohmic, activation, and concentration polarizations, the cell voltage can be found using Eq. (16). Then, we can calculate the power density of the cell, and the electrical efficiency of the cell as shown in Eqs. (22) and (23).

$$\dot{W}_{cell}'' = j\cdot V \tag{22}$$

$$\eta_{el} = \frac{\dot{W}_{cell}''}{\dot{N}_{1,CH_3OH}''\cdot \overline{LHV}} \tag{23}$$

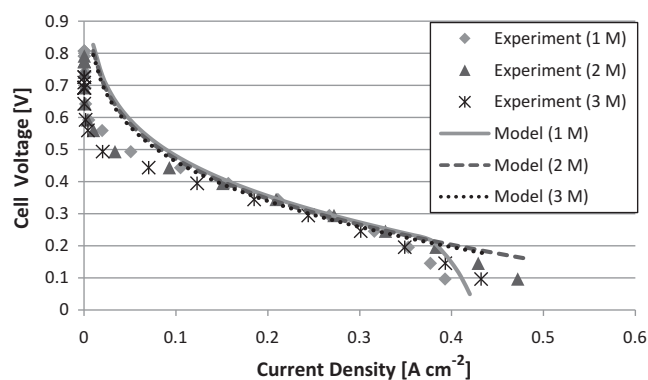**Fig. 4.** Validation of the DMFC model for different methanol concentrations at the feed stream ($T = 70\,^\circ$C).

If the flowing electrolyte is circulated, the electrical efficiency can be shown as follows:

$$\eta_{el} = \frac{\dot{W}''_{cell}}{[\dot{N}''_{1,CH_3OH} - (\dot{N}''_{3,CH_3OH} - \dot{N}''_{5,CH_3OH})] \cdot \overline{LHV}} \quad (24)$$

3. Results and discussion

In this section, the validation of the model given in Section 2 is first presented. Then, the results of the simulations for the effects of the electrolyte flow rate, flowing electrolyte channel thickness, methanol concentration at the feed stream, and circulation of the flowing electrolyte on the performance of a single cell are discussed. The input data used in the calculations are shown in Table 2. It should be noted that some input data that vary in the simulations are shown within the figures.

3.1. Validation

Experimental results obtained by Ge and Liu [25] were used to validate the DMFC model developed. These experiments were carried out on a liquid fed DMFC at different operating temperatures, methanol concentrations, anode flow rates, air flow rates, and cathode humidifications. The materials used for the cell were as follows: Nafion® 117 for the membrane, carbon cloth for the anode and cathode backing layers, Pt–Ru with a loading 3 mg cm^{-2} for the anode catalyst layer, and Pt-black with a loading of 3 mg cm^{-2} for the cathode catalyst layer. The thicknesses of the backing layers and the membrane, as well as the porosities of the components used in these experiments and the simulations of the current study are shown in Table 2. The other input parameters of the simulations are chosen to give the best fit with the experimental data after a comparative search from the literature.

The results of the simulations for different methanol concentration at the feed stream, such as 1 M, 2 M, and 3 M, were compared with the experimental data. In these simulations, the cell temperature was taken as 70 °C. In addition, since the flow rates of air and anode inlet are not input data because of the limitations of the 1D model, the highest values of these parameters used in the experiments, which are 6 ml min^{-1} for methanol and 1200 sccm for air, were considered for validation. The number of nodes in the flowing electrolyte channel was taken as 100 in the simulations after conducting a grid convergence study. The results of the comparison of the simulations with the experimental data are shown in Fig. 4. As can be seen in this figure, the simulation results are in good agreement with the experimental data, especially at the region where the current density is higher than 0.1 A cm^{-2}. The discrepancy in the low current density should be related to using Tafel law, which is valid when the cell 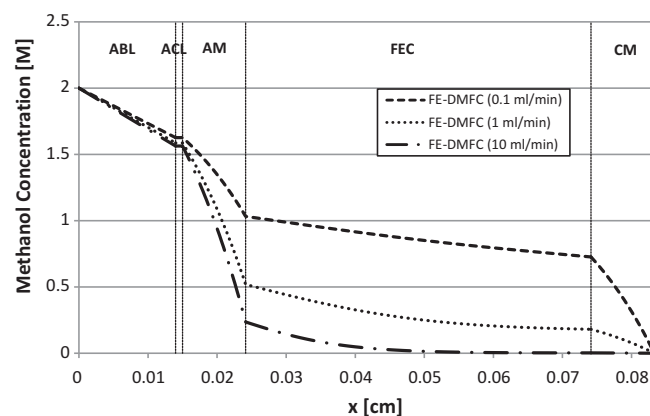current density is higher than the exchange current density. Since we could not get data below the exchange current density, we cannot have a meaningful comparison for low current density conditions. For the current densities higher than 0.38 A cm^{-2}, the trend of the polarization curves also differs slightly. This difference might be due to considering only liquid phase at the anode. However, in reality, CO_2 bubbles and H_2O vapour affect the limiting current density.

3.2. Effect of electrolyte flow rate

Electrolyte flow rate is one of the most important input parameters affecting the performance of a FE-DMFC. Depending on this flow rate, amount of methanol reaching the CCL changes, hence the crossover current density, cathodic activation polarization, cell voltage, and power density of the cell are affected. Since our aim is to eliminate the methanol crossover completely to increase the performance of the cell, we have studied the effect of this parameter on the output parameters and identified the value of this parameter that ensures zero methanol crossover.

Figs. 5 and 6 show the methanol concentration through the different layers of the cell in the thickness direction for various electrolyte flow rates (0.1 ml min^{-1}, 1 ml min^{-1}, and 10 ml min^{-1}) at a low current density (0.1 A cm^{-2}) and a high current density (0.4 A cm^{-2}) condition, respectively. In these simulations, the temperature, methanol concentration at the feed stream, and thickness of the flowing electrolyte channel are taken as 80 °C, 2 M, and 0.05 cm, respectively. These figures show that as we increase the electrolyte flow rate, the methanol concentration reaching the CCL
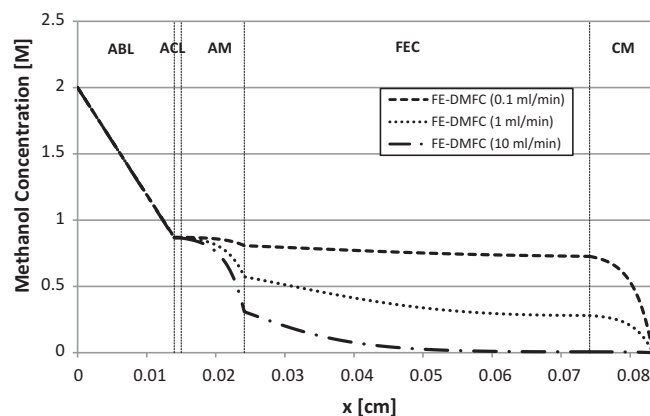

Fig. 5. Methanol concentration distribution in a FE-DMFC at $j = 0.1$ A cm^{-2} for different electrolyte flow rates ($T = 80\,^\circ$C, $C_{MeOH} = 2$ M, and $t_{FEC} = 0.05$ cm).

Fig. 6. Methanol concentration distribution in a FE-DMFC at $j = 0.4$ A cm^{-2} for different electrolyte flow rates ($T = 80\,^\circ$C, $C_{MeOH} = 2$ M, and $t_{FEC} = 0.05$ cm).

Table 2
Input data.

Input parameter	Value
Thickness of the anode backing layer	0.014 cm [15]
Thickness of the anode catalyst layer	0.001 cm [12]
Thickness of the membrane (DMFC)	0.0183 cm [21]
Thickness of the anode membrane (FE-DMFC)	0.0092 cm (assumed)
Thickness of the cathode membrane (FE-DMFC)	0.0092 cm (assumed)
Thickness of the cathode catalyst layer	0.001 cm [12]
Thickness of the cathode backing layer	0.014 cm [15]
Width of the active cell	5 cm [10]
Length of the active cell	5 cm [10]
Porosity of the anode backing layer	0.6 [15]
Porosity of the cathode backing layer	0.6 [15]
Porosity of the membranes	0.28 [15]
Porosity of the spacer in the flowing electrolyte channel	0.6 (assumed)
Pressure of the cathode	1 atm
Molar ratio of oxygen in the cathode feed stream	21%
Reference exchange current density of the anode	$94.25 \times 10^{-4} \times e^{[35,570/R \cdot (1/353 - 1/T)]}$ (A cm^{-2}) [16]
Reference exchange current density of the cathode	$0.04222 \times 10^{-4} \times e^{[73,200/R \cdot (1/353 - 1/T)]}$ (A cm^{-2}) [16]
Reference methanol concentration at the anode at 80 °C	10^{-4} mol cm^{-3} [16]
Anodic transfer coefficient	0.239 [16]
Cathodic transfer coefficient	0.875 [16]
Electro-osmotic drag coefficient of water	$1.6767 + 0.0155 \times T + 8.9074 \times 10^{-5} \times T^2$ (T is in °C) [22]
Coefficient of diffusion of methanol at the anode backing layer and flowing electrolyte channel	$\varepsilon^{1.5} \times 2.8 \times 10^{-5} \times e^{[2436 \cdot (1/353 - 1/T)]}$ (cm^2 s^{-1}) [10,23]
Coefficient of diffusion of methanol at the membranes	$\varepsilon^{1.5} \times 4.9 \times 10^{-6} \times e^{[2436 \cdot (1/333 - 1/T)]}$ (cm^2 s^{-1}) [23]
Coefficient of diffusion of oxygen at the cathode backing layer	$\varepsilon^{1.5} \times (T^{1.75} \times 5.8 \times 10^{-4}/(27.772 \times P))$ (cm^2 s^{-1}) [18]
Conductivity of the membrane	0.1 S cm^{-1} [21]
Conductivity of the sulphuric acid solution	1.45 S cm^{-1} [24]

decreases because the methanol carried out from the cell is proportional to the velocity of the electrolyte. It can be observed from Fig. 5 that the main mechanism affecting the methanol concentration distribution is the diffusion since electro-osmosis affect is less at low current densities. When we run the fuel cell at high current densities, the effect of electro-osmosis becomes more significant, as can be seen from Fig. 6.

The change of the crossover current density with the cell current density for different electrolyte flow rates is shown in Fig. 7. For comparison between DMFC and FE-DMFC, the results for DMFC are also added to this figure. For the DMFC case, as the current density increases, the total flow rate of methanol diffusing through the ABL increases, mainly because of the increase in the molar flow rate of methanol spent in the electrochemical reaction. In addition, the methanol crossover due to electro-osmosis also increases, but the methanol crossover due to diffusion decreases. Up to a certain current density, the increase in the methanol crossover due to electro-osmosis is higher than the decrease in the methanol crossover due to diffusion. Hence, the crossover current density increases. However, when the concentration of methanol at the ACL becomes very low, the change of total molar flow rate of methanol diffusing through the ABL with the current density
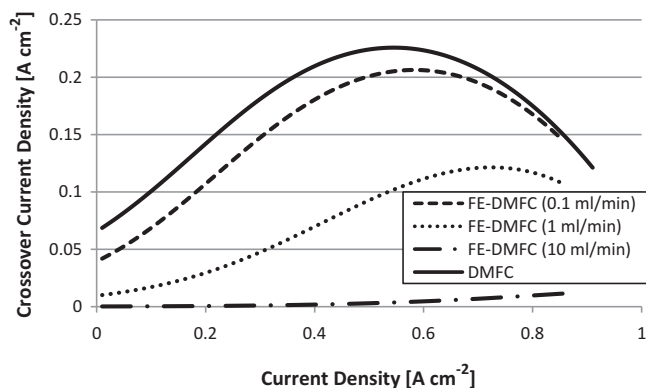
becomes insignificant. At this point, since the molar flow rate of methanol spent in the electrochemical reaction increases, the amount of methanol crossover and the crossover current density decrease. In the case of FE-DMFC, the trends are similar. The main difference is that the peak point of the crossover current density is achieved at higher cell current densities with an increase in the electrolyte flow rate. As can be followed from Fig. 7, even a small rate of electrolyte, e.g. 0.1 ml min^{-1}, could reduce the crossover current density significantly. The value of this flow rate that makes the crossover current density zero also depends on the current density that the fuel cell operates. For example, even at 10 ml min^{-1}, this value is slightly higher than zero for high current density conditions, which can be seen in Fig. 7. The results of our simulation show that when the electrolyte flow rate is 26 ml min^{-1}, the crossover current density becomes less than 10^{-3} for any cell current density conditions.

In a DMFC, the mixed potential occurs at the cathode because of the combined effect of the voltage loss due to the slow reaction rate, and the crossover polarization due to the reduction of active areas and molar fraction of oxygen caused by the oxidation of methanol at the CCL. Here, we can define the crossover polarization as the difference between the cathodic activation polarizations of a FE-DMFC at any given condition and a FE-DMFC operating at a condition that ensures negligible methanol crossover to the cathode side. This crossover polarization can be eliminated in a FE-DMFC when the electrolyte flow rate is taken high enough such as 10 ml min^{-1}, as can be seen in Fig. 8. As the electrolyte flow rate decreases, the crossover polarization increases, and reaches its maximum value when the electrolyte flow rate becomes zero. At this condition, the cathodic activation polarization of the FE-DMFC becomes same as that of the DMFC. In addition, the open circuit voltage (OCV) becomes equal to the reversible OCV, i.e., 1.21 V, for zero crossover polarization. However, since we use the Tafel law in our modeling, the initial current density must be taken as the exchange current density. Due to this reason, the cathodic activation polarization is shown higher than zero, i.e., 0.27 V, for the initial current density, i.e., 0.01 A cm^{-2}, when the methanol crossover becomes negligible.

The effects of electrolyte flow rate on the cell voltage and power density of the cell are shown in Figs. 9 and 10, respectively. As
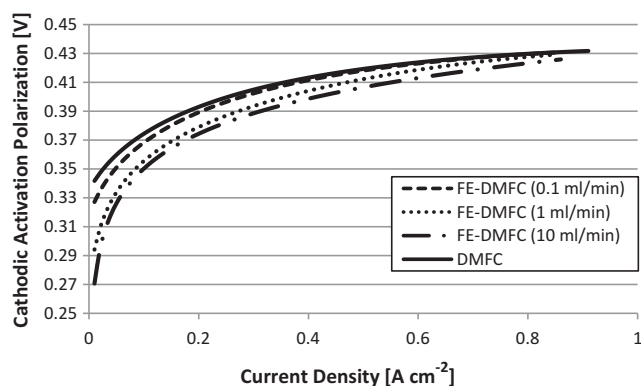
Fig. 7. Change of crossover current density with cell current density for different electrolyte flow rates ($T = 80$ °C, $C_{MeOH} = 2$ M, and $t_{FEC} = 0.05$ cm).

Fig. 8. Change of cathodic activation polarization with cell current density for different electrolyte flow rates ($T = 80\,^\circ$C, $C_{MeOH} = 2$ M, and $t_{FEC} = 0.05$ cm).
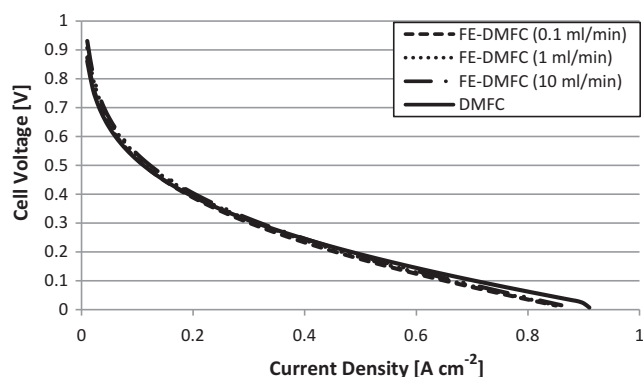

Fig. 9. Change of cell voltage with cell current density for different electrolyte flow rates ($T = 80\,^\circ$C, $C_{MeOH} = 2$ M, and $t_{FEC} = 0.05$ cm).

expected, these output parameters become maximum for a FE-DMFC when the methanol crossover is completely eliminated. When we compare the performance of a DMFC with FE-DMFC operating with 10 ml min^{-1} electrolyte flow rate, the performance of a FE-DMFC is better at current densities lower than 0.41 A cm^{-2}; and that of a DMFC is better at current densities higher than this value. This finding can be explained as follows: when we use a FE-DMFC instead of a DMFC at low current densities, the gain from the reduction of methanol crossover or cathodic activation polarization is higher than the loss from the ohmic polarization increase due to the addition of the flowing electrolyte channel for a FE-DMFC. On the other hand, the ohmic polarization at the flowing electrolyte channel increases significantly at high current densities, hence the
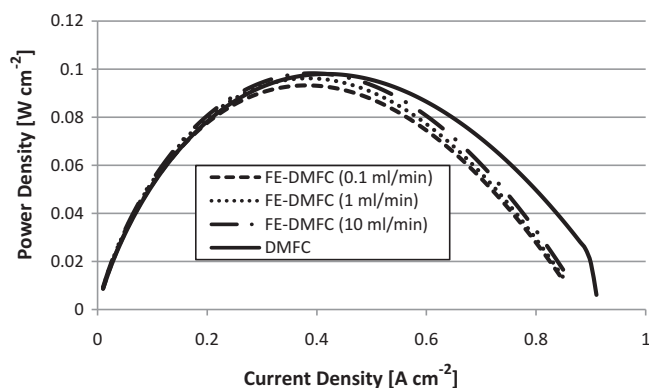

Fig. 10. Change of power density the cell with cell current density for different electrolyte flow rates ($T = 80\,^\circ$C, $C_{MeOH} = 2$ M, and $t_{FEC} = 0.05$ cm).
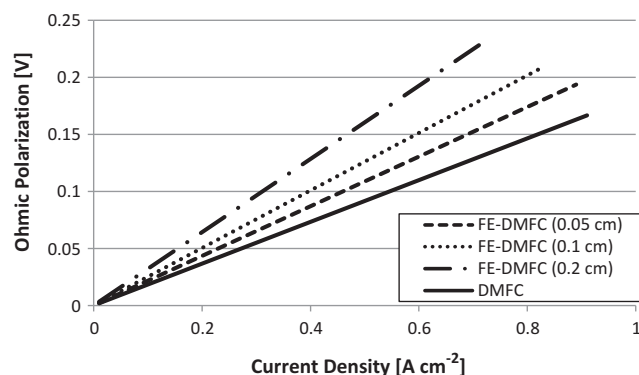

Fig. 11. Effect of the thickness of flowing electrolyte channel on the ohmic polarization for zero cross-over current density conditions ($T = 80\,^\circ$C, $C_{MeOH} = 2$ M).

performance of FE-DMFC drops at these conditions. The ohmic polarization change with current density is explained in detail in the next section. When we compare the maximum power densities of these fuel cells, we find that the value of this power density for FE-DMFC for 10 ml min^{-1} electrolyte flow rate (98.05 mW cm^{-2}) is slightly higher than that for DMFC (97.9 mW cm^{-2}). It should also be noted that the effect of the additional power demand of the flowing electrolyte pump has been considered in this comparison. We found that this demand is negligible for the electrolyte flow rates considered; and it has no significant effect on the performance of the cell. The results of a previous work [9] also confirm our finding on the effect of this power demand. The flowing electrolyte rate has also no effect in the electrical efficiency of a FE-DMFC since we assume that the methanol and sulfuric acid leaving the cell can be separated and then recirculated. A comparison on the cell efficiencies of DMFC and FE-DMFC are given in Section 3.5.

3.3. Effect of flowing electrolyte channel thickness

The determination of the flowing electrolyte channel thickness is another important design parameter for FE-DMFCs. The effect of this thickness on the performance of the FE-DMFC is investigated at a cell temperature of 80 $^\circ$C and a methanol feed concentration of 2 M. From the results and discussion of the previous section, it should be expected that increasing the thickness of a flowing electrolyte channel at a given electrolyte flow rate will decrease the methanol crossover. However, as we found that the flowing electrolyte pump work is negligible, we can adjust the electrolyte flow rate high enough for any electrolyte channel thickness, and eliminate the methanol crossover without any changes in the performance. Thus, the effect of flowing electrolyte channel thickness is studied for the conditions ensuring no methanol crossover, i.e., zero crossover current density conditions.

The change in flowing electrolyte channel thickness for a FE-DMFC operating at high enough electrolyte flow rates mainly affects the ohmic polarization of the cell. Fig. 11 shows the ohmic polarization for a FE-DMFC at flowing electrolyte channel thicknesses of 0.05 cm, 0.1 cm, and 0.2 cm as well as that for a DMFC. When we neglect the contact resistances and losses due to the electron flow at the external loop, this polarization mainly occurs due to the flow of protons through the anode membrane, flowing electrolyte channel, and cathode membrane. For the comparison shown in Fig. 11, the change in the total ohmic polarization of a FE-DMFC with the thickness of the flowing electrolyte channel is only due to the changes of this polarization at this channel. In addition, as we considered the total thickness of the anode and cathode membranes of a FE-DMFC equal to the thickness of the membrane of the DMFC, the ohmic polarization change in this channel is also the only effective factor in the comparison between these fuel cells. Considering that this
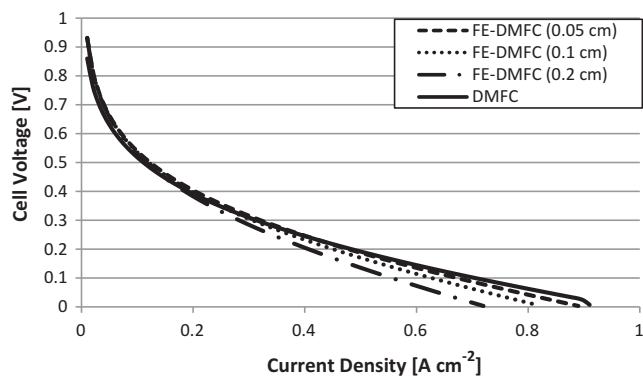
Fig. 12. Effect of the thickness of flowing electrolyte channel on the cell voltage for zero cross-over current density conditions ($T = 80\,°C$, $C_{MeOH} = 2\,M$).

voltage loss obeys the Ohm's law, we found that the thickness of this channel should be taken as low as possible. The minimum thickness that could be taken is considered as 0.5 mm taking into account the discussions of a previous study [7]. It should also be noted that the conductivity of the sulfuric acid changes significantly with temperature and concentration. Hence, we chose the concentration that will maximize the conductivity of H_2SO_4 at a given temperature, i.e., conductivity of $1.45\,S\,cm^{-1}$ at 36% by weight and $80\,°C$ [24].

The effects of the flowing electrolyte channel thickness on the cell voltage and power density of a DMFC and FE-DMFC are shown in Figs. 12 and 13, respectively. As the ohmic polarization is higher for thicker electrolyte channels, the performance gets lower for these conditions. In addition, as the total thickness of a single cell increases for thicker channels; the volumetric power density of the system decreases.

3.4. Effect of methanol concentration at the feed stream

Methanol concentration at the feed stream should be controlled in a DMFC to reduce the effects of the methanol crossover. Since the entire methanol is assumed to be spent at the CCL, if we increase the methanol concentration at the feed stream above a certain value, both the concentration difference of methanol across the membrane and molar flow rate of methanol reaching the CCL increase. This increase leads to a higher crossover current density and cathodic activation polarization; hence the performance of the cell deteriorates. The cell voltage and power density of a DMFC operating at $80\,°C$ are shown in Figs. 14 and 15, respectively. As can be seen from these figures, the maximum power density of the cell is achieved when the methanol concentration is around 1 M. At this condition, the value of the current
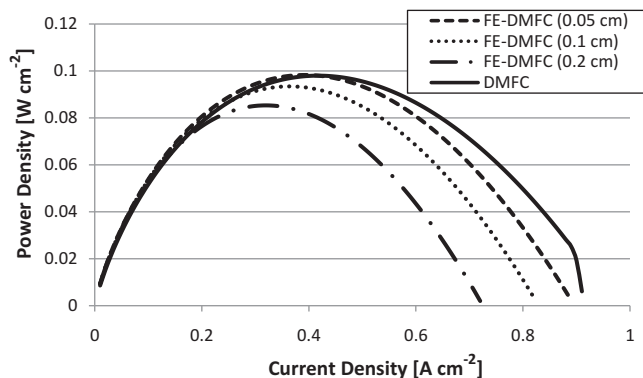

Fig. 13. Effect of the thickness of flowing electrolyte channel on the power density of the cell for zero cross-over current density conditions ($T = 80\,°C$, $C_{MeOH} = 2\,M$).
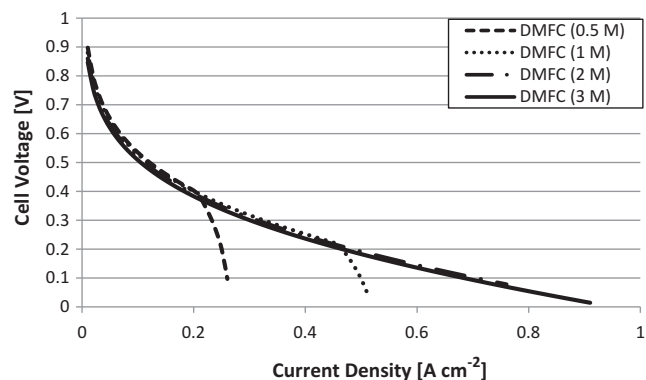

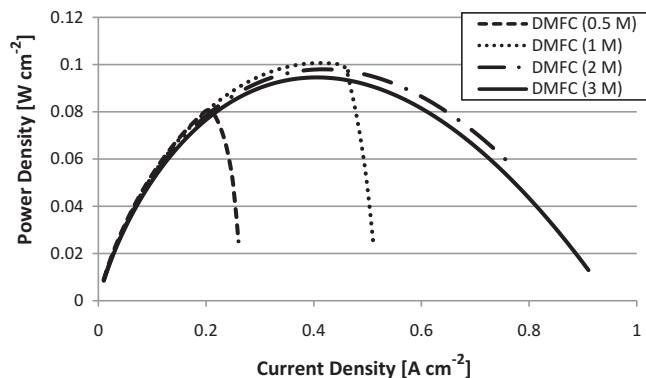**Fig. 14.** Effect of concentration of the methanol at the feed stream on the cell voltage of the DMFC ($T = 80\,°C$).

Fig. 15. Effect of concentration of the methanol at the feed stream on the power density of the DMFC ($T = 80\,°C$).

density and power density are $0.41\,A\,cm^{-2}$ and $0.1\,W\,cm^{-2}$, respectively.

The changes of the cell voltage and power density of a FE-DMFC, which operates at $80\,°C$ and at no methanol crossover conditions, with methanol concentration at the feed stream are shown in Figs. 16 and 17, respectively. It can be seen from these figures that the trend of these curves for a FE-DMFC is different than those for a DMFC. In a FE-DMFC, the maximum power density increases as we increase the methanol concentration up to a certain value; and after this value, there is no change in the performance of the cell. This trend occurs due to the fact that the all the methanol is carried away from the cell in the FE-DMFC studied; hence cathodic activation polarization does not change with an increase in the methanol
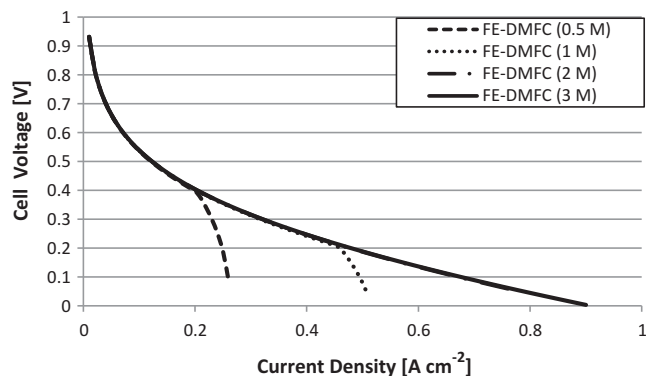

Fig. 16. Effect of concentration of the methanol at the feed stream on the cell voltage of the FE-DMFC for zero cross-over current density conditions ($T = 80\,°C$, $t_{FEC} = 0.05\,cm$).
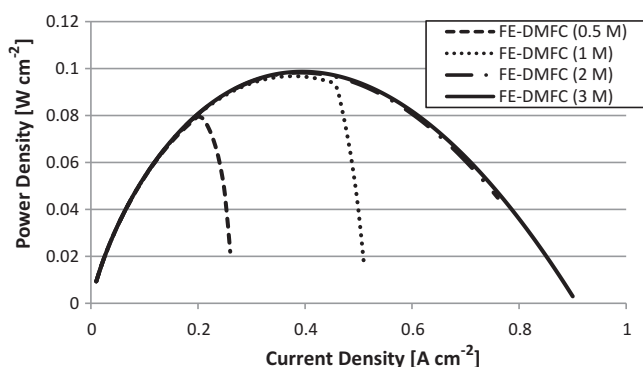
Fig. 17. Effect of concentration of the methanol at the feed stream on the power density of the FE-DMFC for zero cross-over current density conditions (T = 80 °C, t_{FEC} = 0.05 cm).

concentration. Fig. 17 shows that the maximum power density is achieved when the methanol concentration at the feed is stream is around 2 M. At this concentration, the values of the current density and power density are approximately 0.41 A cm^{-2} and 0.1 W cm^{-2}, respectively. On the other hand, these results have showed that concentrated methanol could be used without any performance drop in a FE-DMFC. This usage could provide some advantages such as a decrease in the methanol cartridge size or an increase in the operation time of the system with a given cartridge.

3.5. Effect of circulation of the flowing electrolyte

In a DMFC, the methanol crossing over through the membrane is completely oxidized at the CCL; hence there is no possibility to recover this methanol. However, in a FE-DMFC, the methanol crossing over through the cell is washed away by the electrolyte flow; and then it could be recovered and circulated. The detailed schematic and discussions on this circulation loop can be found in the paper of Kordesch et al. [5]. This circulation reduces the amount of methanol required at a given time when the system is at steady-state; hence the electrical efficiency of the cell increases; which can be seen in Fig. 18. If we compare the cell efficiencies of a DMFC and a FE-DMFC for the maximum power density conditions, we can see that FE-DMFC with re-circulation (C-FE-DMFC) has an efficiency of 22%; whereas DMFC has an efficiency of 14%. This shows that we can increase the efficiency of a DMFC by 57% when we replace it with a FE-DMFC. However, the additional components related to this circulation loop cause an increase in the system size; which limits the application areas of the FE-DMFC.
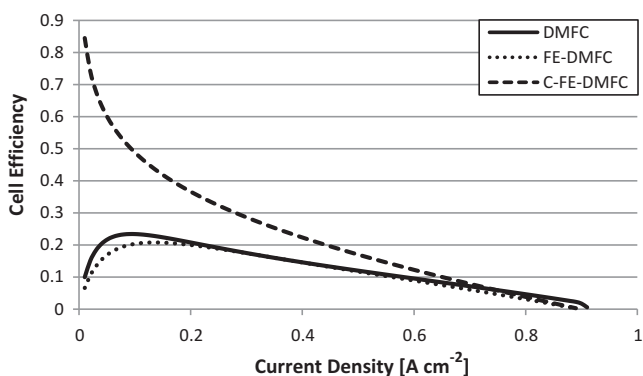

Fig. 18. Electrical efficiency of the cell for DMFC, FE-DMFC, and C-FE-DMFC (T = 80 °C, C_{MeOH} = 2 M, and t_{FEC} = 0.05 cm, zero cross-over current density for FE-DMFC and C-FE-DMFC).

4. Conclusions

The feasibility of using the FE-DMFC instead of the DMFC in portable power application has been investigated through a modeling study. For this purpose, models for DMFC and FE-DMFC have been developed by integrating the water, methanol, and oxygen transport equations with electrochemical relations. These models give the concentrations distribution of the species, cell voltage, power density and cell efficiency as the output. After validating the model with the literature data, several simulations have been carried out to analyze the effects of the input parameters on the cell performance, and to identify the parameters that maximize the performance of the cell. The main findings of these simulations are listed below:

- the electrolyte flow rate should be taken high enough to eliminate the methanol crossover in a FE-DMFC completely; this increases the cell voltage and power density of the cell;
- the additional power input to the flowing electrolyte pump has no significant effect on the performance of the cell;
- the flowing electrolyte channel thickness should be as low as possible to minimize the ohmic losses in the flowing electrolyte channel;
- highly concentrated methanol can be used in a FE-DMFC without causing any deterioration in the performance of the cell;
- circulating the flowing electrolyte leads to a significant increase on the electrical efficiency of the cell; and
- for the input data considered in this study, the maximum power densities of the DMFC and FE-DMFC are both found approximately as 0.1 W cm^{-2}, but the electrical efficiency of the circulated FE-DMFC is found to be 57% more than that of the DMFC.

This study suggests that FE-DMFCs can provide much better electrical cell efficiencies compared to DMFCs; however FE-DMFCs are limited in terms of application areas since the system size gets bigger for this fuel cell type. For future work, a new model will be developed considering the multi-dimensional and multi-phase effects and the effect of membrane type as well as other operating parameters on the performance of FE-DMFCs will be investigated.

References

[1] C.O. Colpan, I. Dincer, F. Hamdullahpur, in: S. Kakac, A. Pramuanjaroenkij, L. Vasiliev (Eds.), Mini-Micro Fuel Cells: Fundamentals and Applications. NATO Science for Peace and Security Series, Springer, Netherlands, 2008, pp. 87–101.
[2] C.Y. Wang, in: S. Kakac, A. Pramuanjaroenkij, L. Vasiliev (Eds.), Mini-Micro Fuel Cells: Fundamentals and Applications. NATO Science for Peace and Security Series, Springer, Netherlands, 2008, pp. 235–242.
[3] K. Kordesch, M. Cifrain, T. Hejze, V. Hacker, U. Bachhiesl, Proceedings of the Fuel Cell Seminar 2000, Portland, OR, USA, October 30 – November 2, 2000, pp. 432–435.
[4] K. Kordesch, V. Hacker, Proceedings of the 17th International Electric Vehicle Symposium & Exhibition, Montreal, QC, Canada, October 15–18, 2000.
[5] K. Kordesch, V. Hacker, U. Bachhiesl, Journal of Power Sources 96 (2001) 200–203.
[6] News, Fuel Cells Bulletin (March) (2004) 9.
[7] D. James, S.-J. Xia, Y. Shen, D. Toolsie, K. Kordesch, N. Beydokhti, 2003 Fuel Cell Seminar, Miami, FL, November 3-7, 2003.
[8] T. Schaffer, V. Hacker, J.O. Besenhard, Journal of Power Sources 153 (2006) 217–227.
[9] E. Kjeang, J. Goldak, M.R. Golriz, J. Gu, D. James, K. Kordesch, Fuel Cells 4 (2005) 486–498.
[10] E. Kjeang, J. Goldak, M.R. Golriz, J. Gu, D. James, K. Kordesch, Journal of Power Sources 153 (2006) 89–99.

[11] Carleton MAE Fuel Cell Project. http://fuelcell.mae.carleton.ca/ (accessed 23.08.2010).
[12] A.A. Kulikovsky, in: T.S. Zhao, K.D. Kreuer, T.V. Nguyen (Eds.), Advances in Fuel Cells, vol. 1, Elsevier, 2007, pp. 337–417.
[13] F. Liu, G. Lu, C.Y. Wang, Electrochemical and Solid-State Letters 8 (1) (2006) A1–A4.
[14] C.Y. Wang, in: S. Kakac, A. Pramuanjaroenkij, L. Vasiliev (Eds.), Mini-Micro Fuel Cells: Fundamentals and Applications. NATO Science for Peace and Security Series, Springer, Netherlands, 2008, pp. 243–256.
[15] J. Ge, H. Liu, Journal of Power Sources 160 (2006) 413–421.
[16] Z.H. Wang, C.Y. Wang, Journal of the Electrochemical Society 150 (4) (2003) A508–A519.
[17] B.L. Garcia, V.A. Sethuraman, J.W. Weidner, R.E. White, R. Dougal, Journal of Fuel Cell Science and Technology 1 (November) (2004) 43–48.
[18] V.B. Oliveira, D.S. Falcao, C.M. Rangel, A.M.F.R. Pinto, International Journal of Hydrogen Energy 33 (2008) 3818–3828.
[19] F.M. White, Fluid Mechanics, 5th ed., McGraw-Hill, Boston, 2003.
[20] J. Larminie, A. Dicks, Fuel Cell Systems Explained, 2nd ed., John Wiley, UK, 2003, pp. 157–158.
[21] DuPont Fuel Cells, http://www2.dupont.com/FuelCells/en_US/products/literature.html (accessed 23.08.2010).
[22] G. Lu, C.Y. Wang, in: B. Sunden, M. Faghri (Eds.), Transport Phenomena in Fuel Cells, WIT Press, 2005, pp. 317–350.
[23] K. Scott, W. Taama, J. Cruikshank, Journal of Power Sources 65 (1997) 159–171.
[24] H.E. Darling, Journal of Chemical and Engineering Data 9 (3) (1964) 421–426.
[25] J. Ge, H. Liu, Journal of Power Sources 142 (2005) 56–69.